An Analytical Framework for the Performance Evaluation of Node- and Network-Wise Operation Scenarios in Elastic Optical Networks

Hamzeh Beyranvand, Martin Maier, *Senior Member, IEEE*, and Jawad A. Salehi, *Fellow, IEEE*

***Abstract*—In this paper, we analyze the exact node- and network-wise operation scenarios in elastic optical networks (EONs). First, the busy/idle patterns of optical spectrum in a stand-alone node are modeled by utilizing a continuous Markov chain. In the node-wise perspective, four operation scenarios are investigated, which are determined based on the spectrum allocation methods. We present an algorithmic procedure to derive the global balance equations of the corresponding Markov chains for all operation scenarios. Furthermore, the network-wise operation is assessed by analyzing the end-to-end blocking probability for two operation modes, with and without spectrum conversion capabilities at the intermediate nodes. Because the computational complexity of exact model increases exponentially versus the number of spectrum slots, we present two approximate alternatives. The results of the exact models, approximations, and verifying simulations are compared for small scale problem. Comparison reveals that the exact model and simulation match very well. In addition, the accuracy of both approximations is acceptable. The approximate solutions are also examined under large scale scenarios by considering simulation results as a benchmark. The accuracy of the first approximation is not degraded in large scale cases, as opposed to the second one, which is only applicable to small scale problems.**

***Index Terms*—Bandwidth fragmentation ratio (BFR), blocking probability, contiguous spectrum assignment (CSA) constraint, elastic optical networks (EONs), routing and spectrum assignment (RSA).**

I. Introduction

ELASTIC optical networks (EONs) and multi-granular optical networks are attracting much attention as a promising solution to support heterogeneous and bandwidth-hungry applications [1-4]. Optical orthogonal frequency division multiplexing (OFDM) has been considered a viable technique to realize EONs, giving rise to so-called Spectrum-Sliced Elastic Optical Path Networks (SLICE) [1]. One of the main features of SLICE networks is that the optical bandwidth is sliced into overlapped orthogonal subcarriers (OFDM subcarriers) and the assigned bandwidth is adapted with respect to the user's demand. Hence, the spectral utilization efficiency is improved because of the "just-enough" bandwidth allocation, the elimination of the bandwidth mismatch between the user's demand and the available spectrum grids, and the reduction of the spectrum guard bandwidth [1]. In contrast, conventional wavelength division multiplexing (WDM) networks are restricted by the fixed bandwidth per channel determined by the ITU-T G.694 grid spacing.

Although there are some similarities between conventional WDM and EONs, the elasticity and flexibility properties of EONs raise some new issues. In EONs, the assigned optical spectrum is tailored with respect to the requested bit rate, transmission distance, and modulation format. Furthermore, multiple channels can be assigned to accommodate high-data-rate lightpaths, whereby the allocated channels are contiguous. These properties of EONs impose new challenges from the network planning and resource provisioning point of view. In the literature, many studies have been conducted during the last three years to address the routing and spectrum assignment (RSA) problem in EONs [5-11]. The RSA problem in EONs is analogous to the well-known routing and wavelength assignment (RWA) problem in conventional wavelength-routed WDM core networks [12]. However, due to the new features of EONs, conventional RWA algorithms are not directly applicable. Recently, both static and dynamic RSA have been addressed, whereby static RSA is for the network designing or planning phase [5-7] while dynamic RSA is applied during the operational phase, when new lightpath requests should be served [8-11].

Bandwidth fragmentation and physical layer impairments are further key issues of EONs. The use of elastic bandwidth channels can result in spectral fragmentation, which increases the blocking probability and limits the overall network capacity. In addition, variable bandwidth lightpaths and overlapped subcarriers in EONs render them more susceptible to physical layer impairments [13-17]. In [13-15], an adaptive quality-of-transmission (QoT) restoration scheme combining the methods of lightpath rerouting and modulation-format switching has been proposed and experimentally demonstrated to overcome real-time impairments in EONs. Yang and Kuipers [16] presented an impairment-aware RSA solution for translucent EONs, where signal impairments are compensated by means of regeneration at selectively placed regenerators. In [17], a

Manuscript received October 5, 2013; revised January 27 and March 10, 2014. The editor coordinating the review of this paper and approving it for publication was W. Kwong.

This work was supported in part by the Iran Telecom Research Center (ITRC) and the Iran National Science Foundation (INSF), and in part by NSERC Discovery Grant No. 327320-2011.

H. Beyranvand and J. A. Salehi are with the Department of Electrical Engineering, Sharif University of Technology, Tehran, Iran (e-mail: beyranvand@ee.sharif.edu, jasalehi@sharif.edu). Currently, H. Beyranvand is a visiting researcher with the Optical Zeitgeist Laboratory, Institut National de la Recherche Scientifique (INRS), Montréal, QC H5A 1K6, Canada.

M. Maier is with the Optical Zeitgeist Laboratory, Institut National de la Recherche Scientifique (INRS), Montréal, QC H5A 1K6, Canada (e-mail: maier@emt.inrs.ca).

Digital Object Identifier 10.1109/TCOMM.2014.032914.130777

QoT-aware RSA algorithm has been proposed, which allocates the modulation level and spectrum by estimating the QoT of the network via a closed-form expression for physical layer impairments.

The analytical performance evaluation of EONs has begun only recently [2], [11], [18-19]. It is important to note that the methods utilized to analyze traditional WDM networks are not applicable to assess the performance of EONs. In [11], the blocking probability of EONs has been evaluated for three different spectrum allocation policies under time-varying traffic assumptions. The authors have obtained the blocking probability of the dedicated-spectrum allocation policy by using the Erlang formula and approximately calculated the blocking probability of the two shared-spectrum policies by employing some relaxation assumptions [11]. In [18], an iterative procedure has been introduced to estimate the blocking performance of EONs. The authors approximated the bandwidth utilization ratio in order to obtain the blocking probability, then they compared the blocking probability of two scenarios, with and without spectrum conversion. In [19], the blocking probability of a stand-alone EON node was evaluated by modeling the bandwidth occupation as a continuous Markov chain under the first-fit (FF) and random-fit (RF) spectrum assignment approaches. The authors were only able to obtain the general form of the global balance equations (GBEs) of the model, while the details of the model were not explained. Recently, Shi *et al.* investigated the effect of bandwidth fragmentation on the blocking probability of EONs by using a simplified model of the EON operation [2]. To the best of our knowledge, there doesn't exist any unified performance evaluation frameworks to analyze the exact operation of EONs from both the node- and network-wise perspective.

In this work, we model the exact node- and network-wise operation scenarios in EONs. The considered system model is described in Section II. The node-wise performance modeling is presented in Section III. In this section, the bandwidth busy/idle status in a EON node is modeled by utilizing a continuous Markov chain. In the node-wise perspective, four operation scenarios are investigated, which are determined based on the allocation method (FF or RF) and the status of assignment constraint, with or without contiguous spectrum assignment (CSA) constraint. We present an algorithmic procedure to derive the GBEs of the corresponding Markov chains of all operation scenarios. After computing the steady-state probabilities of the bandwidth usage in a node, we evaluate the blocking probability and bandwidth fragmentation ratio in each EON link. In Section IV, the network-wise operation is assessed by analyzing the end-to-end blocking probability for two operation modes, with and without spectrum conversion capability at intermediate nodes. Section V is devoted to present two approximate solutions to obtain the node- and network wise blocking probability. We compare the results of exact models, approximations, and verifying simulations in Section VI. Finally, conclusions are drawn in Section VII.

II. System Description

Unlike conventional WDM networks with a typical grid size of 50 GHz, in EONs the optical spectrum is sliced into slots with grid size of 6.25 GHz or 12.5 GHz [8]. Then, the spectra allocated to the lightpath requests are adapted with respect to the demanded transmission rate and the determined modulation format. It is noted that the modulation format is determined based on the transmission distance of the lightpath and the necessary QoT specified according to the desired bit error rate [17]. The high-data-rate requests are allocated a number of slots, whereby under the CSA constraint these slots must be contiguous, otherwise any available idle slots can be assigned to the high-rate lightpaths. Furthermore, the idle slots can be allocated according to the FF and RF methods, whereby in the FF method, the first idle spectra are assigned to the request, whereas in the RF method idle spectra are randomly selected among the available spectra. Fig. 1 illustrates the different spectrum assignment scenarios. Accordingly, there are four operation scenarios in the node-wise performance evaluation:

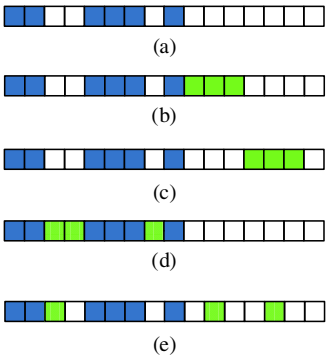

Fig. 1. (a) The initial spectrum occupation state, (b) FF with CSA constraint, (c) RF with CSA constraint, (d) FF without CSA assignment, (e) RF without CSA assignment.

- with CSA constraint and FF assignment (WCSA-FF),
- with CSA constraint and RF assignment (WCSA-RF),
- without CSA constraint and FF assignment (WOCSA-FF),
- without CSA constraint and RF assignment (WOCSA-RF).

It is worthwhile mentioning that in addition to the FF and RF methods, some alternatives have been introduced in [20]. However, in this paper we concentrate on the FF and RF methods as the most used candidates.

From the network layer point of view, there are two scenarios for spectrum assignment depending on the spectrum conversion capability of intermediate routers, with and without spectrum conversion (WSC and WOSC) [18]. Therefore, the operation modes in the network-wise performance evaluation are denoted as follows:

- with spectrum conversion and WCSA-FF (WSC-WCSA-FF),
- with spectrum conversion and WCSA-RF (WSC-WCSA-RF),
- with spectrum conversion and WOCSA-FF (WSC-WOCSA-FF),
- with spectrum conversion and WOCSA-RF (WSC-WOCSA-RF),
- without spectrum conversion and WCSA-FF (WOSC-

WCSA-FF),
- without spectrum conversion and WCSA-RF (WOSC-WCSA-RF),
- without spectrum conversion and WOCSA-FF (WOSC-WOCSA-FF),
- without spectrum conversion and WOCSA-RF (WOSC-WOCSA-RF).

The number of required frequency slots (N_f) is determined as $N_f = \left\lceil \frac{\frac{R}{m}+\Delta G}{\Delta F} \right\rceil$, where R denotes the requested transmission rate, m is the modulation level, ΔG indicates the frequency guard band, and ΔF denotes the grid size of the EON spectrum. It should be noted that the modulation level m denotes 2^m quadratic amplitude modulation (2^m-*QAM*) utilized to modulate the OFDM subcarriers, where m=1,..., 6.

III. Modeling the Node-Wise Operation of EONs

We model the bandwidth busy/idle status in an EON node by using the continuous-time Markov chain proposed in [19], where the states of the Markov chain indicate the number of users and the patterns of busy/idle spectra. In this section, we explain the details of this model and propose an algorithm to derive its GBEs. In our notation, users are classified according to the number of required spectrum slots, whereby a user who needs i slots is assigned to the i-th class. Thus, the user classification in this paper is different from the common terminology in multi-class service networks. We assume that the optical spectrum is sliced into C slots and there are K classes of users. Let vector n=(n_1, n_2, ..., n_K) denote the number of users where n_i is the number of class i users. The busy/idle status of spectrum is represented by occupied-spectrum-vector $OSV_{(n,q)}$, where, q is the qth permutation pattern of busy/idle slots for the given n. We define $OSV_{(n,q)} = \{(f_{L(1)}, f_{U(1)}), (f_{L(2)}, f_{U(2)}), ..., (f_{L(N_n)}, f_{U(N_n)})\}$, where $f_{L(j)}$ and $f_{U(j)}$ are the lower and upper frequency of the jth busy spectrum interval with bandwidth of $\Delta BW_j = (f_{U(j)} - f_{L(j)})$, respectively, and $N_n = \sum_{i=1}^{K} n_i$ is the total number of established lightpaths for a given n. If $\Delta BW_i = j\Delta F$, then the ith occupied spectrum is in the class j, where ΔF is the grid size of spectrum slots. In Fig. 1(a), for example, we have C=16 and by assuming K=3, the OSV of this spectrum pattern is $\{(0, 2\Delta F), (4\Delta F, 7\Delta F), (8\Delta F, 9\Delta F)\}$ and $n = (1, 1, 1)$. Henceforth, for the sake of simplicity and without loss of generality we remove the term ΔF from the OSV representation.

It is worthwhile pointing out that the total number of busy/idle patterns in the operation scenarios with and without the CSA constraint, $N_{WCSA}(n)$ and $N_{WOCSA}(n)$, for a given n are calculated by counting all the permutations of busy and idle spectra. The number of idle slots are $E = C - \sum_{i=1}^{K} b_i n_i$, where b_i indicates the number of slots assigned to a class i user. Hence, $N_{WCSA}(n)$ is obtained by counting all permutations of E idle slots and $\sum_{i=1}^{K} n_i$ occupied spectra as given in (1a), whereas $N_{WOCSA}(n)$ is calculated by considering the permutations of C idle and occupied slots as given by (1b).

$$N_{WCSA}(n) = \frac{(E + \sum_{i=1}^{K} n_i)!}{E!(\prod_{i=1}^{K} n_i!)}, \tag{1a}$$

$$N_{WOCSA}(n) = \frac{C!}{E!(\prod_{i=1}^{K} n_i!)}. \tag{1b}$$

It should be noted that in WSCA, occupied slots of each class are contiguously permuted, whereas in WOSCA, slots allocated to each class can be noncontiguous. Therefore, there are $\sum_{i=1}^{K} n_i$ and $\sum_{i=1}^{K} b_i n_i$ disjoint occupied spectra in WSCA and WOSCA, respectively, which permute with E idle slots and produce $N_{WCSA}(n)$ and $N_{WOCSA}(n)$ permutations as given by (1). The denominators of (1a) and (1b) decrement the number of the same patterns counted by the numerator due to the same class busy and idle slots. As shown in Fig. 1, the occupation pattern in the case without CSA constraint does not affect the blocking probability, because in this case blocking occurs once the total number of idle slots is less than the demanded slots (N_f), whereas under the CSA constraint a request is served if there are at least N_f contiguous idle slots. For example, considering the spectrum pattern shown in Fig. 1(a), a request with N_f=8 under the CSA constraint is blocked, though it can be served in the scenario without CSA constraint. Furthermore, the spectrum patterns can be categorized with respect to n, then OSVs of each group are numbered based on the permutation patterns. In Appendix A, we present an algorithmic procedure to categorize and index all spectrum patterns for any given C and K.

A. Operation model of a stand-alone EON node with CSA constraint

The steady-state probabilities of the spectrum patterns are necessary to evaluate the performance of EONs. Toward this end, all the possible transitions among states must be determined. As shown in Fig. 2, the transition scenarios depend on the spectrum allocation method, FF or RF. In the RF spectrum allocation, the outgoing rates for class k arrivals and departures are $\frac{\lambda_k}{m_k^+}$ and μ_k, respectively, where λ_k and μ_k are the Poisson arrival and departure rates of a class k user, respectively; and m_k^+ is the number of all scenarios, which can allocate k contiguous idle slots to a class k user. In addition, the incoming rates for class k arrivals and departures are $\frac{\lambda_k}{m_k'^+}$ and μ_k, respectively, where $m_k'^+$ has the same definition as m_k^+, which depends on the pattern of the former states. As shown in Fig. 2(a), we have $m_1'^+ = 4$ and $m_2'^+ = 4$, which denote the number of scenarios to serve an incoming class 1 and class 2 user in the states $OSV_{((n=(0,1,0),4))}$ and $OSV_{((n=(1,0,0),1))}$, respectively. On the other hand, in the FF spectrum assignment, the outgoing and incoming transition rates of arrivals are λ_k, while the transition rates in the case of departures are the same as that of the RF method.

By considering all the possible transitions from/in a spectrum pattern, we can write its GBE. For instance, the GBE of the spectrum pattern depicted in Fig. 2 is given by:

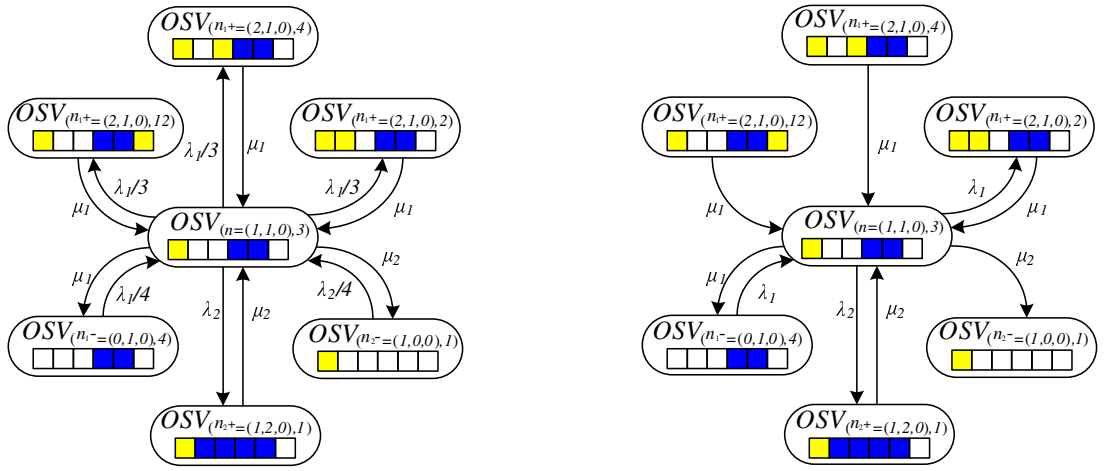

Fig. 2. Transition scenarios of the $OSV_{(n=(1,1,0),3)}$ under the (a) WCSA-RF and (b) WCSA-FF spectrum allocation methods (C=6, K=3).

TABLE I
NOTATIONS

Notation	Description
λ_k	Arrival rate of class k users
μ_k	Average holding time of class k users.
n	$n=(n_1,...,n_K)$, where n_i is the number of class i users.
$OSV_{(n,i)}$	ith spectrum pattern of a given n.
$P\left(OSV_{(n,i)}\right)$	Probability that system is in $OSV_{(n,i)}$.
$n_j^{\pm}$	$\mathrm{n}_j^{\pm}=(n_1,...,n_j\pm1,...,n_K)$.
$\Gamma^{k+}_{OSV_{(n,i)}}$	Set of all possible states after the arrival of a class k user in state $OSV_{(n,i)}$.
$\Gamma^{k-}_{OSV_{(n,i)}}$	Set of all possible states after the departure of a class k user in state $OSV_{(n,i)}$.
$m^{k\pm}_{OSV_{(n,i)}}$	Number of elements in $\Gamma^{k\pm}_{OSV_{(n,i)}}$
$\Omega^{WCSA}_{(C,K)}$	Set of all possible occupation patterns in WCSA operation modes (RF and FF) for the given C and K.

$$
\begin{aligned}
&(\lambda_1+\lambda_2+\mu_1+\mu_2)P(OSV_{(n,3)})=\\
&\mu_1\left(P(OSV_{(n_1^+,2)})+P(OSV_{(n_1^+,4)})+P(OSV_{(n_1^+,12)})\right)+\\
&\mu_2P(OSV_{(n_2^+,1)})+\frac{\lambda_1}{4}P(OSV_{(n_1^-,4)})+\frac{\lambda_2}{4}P(OSV_{(n_2^-,1)}), \qquad (2a)\\
&(\lambda_1+\lambda_2+\mu_1+\mu_2)P(OSV_{(n,3)})=\\
&\mu_1\left(P(OSV_{(n_1^+,2)})+P(OSV_{(n_1^+,4)})+P(OSV_{(n_1^+,12)})\right)+\\
&\qquad\mu_2P(OSV_{(n_2^+,1)})+\lambda_1P(OSV_{(n_1^-,4)}), \qquad (2b)
\end{aligned}
$$

where (2a) and (2b) are the GBE of Fig. 2(a) and Fig. 2(b), respectively. For convenience, the employed notations are summarized in Table I. Generally, the GBEs of each state in both spectrum allocation methods can be obtained by using the following relation:

$$
\begin{aligned}
&\left(\sum_{k=1,\ \Gamma^{k+}_{OSV_{(n,i)}}\neq\emptyset}^{K}\lambda_k+\sum_{k=1,\ \Gamma^{k-}_{OSV_{(n,i)}}\neq\emptyset}^{K}m^{k-}_{OSV_{(n,i)}}\mu_k\right)P(OSV_{(n,i)})\\
&=\sum_{k=1,\ \Gamma^{k+}_{OSV_{(n,i)}}\neq\emptyset}^{K}\left(\sum_{j=1}^{m^{k+}_{(n,i)}}\mu_kP(OSV_{(n_k^+,j)})\right)+\\
&\qquad\sum_{k=1,\ \Gamma^{k-}_{OSV_{(n,i)}}\neq\emptyset}^{K}\left(\sum_{j=1}^{m^{k-}_{(n,i)}}\frac{\lambda_k}{m^{k+}_{OSV_{(n_k^-,j)}}}P(OSV_{(n_k^-,j)})\right),\\
&\qquad\qquad\forall OSV_{(n,i)}\in\Omega^{WCSA}_{(C,K)}. \qquad (3)
\end{aligned}
$$

The derivation of $\Gamma^{k\pm}_{OSV_{(n,i)}}$ and $m^{k\pm}_{OSV_{(n,i)}}$ is not straightforward and depends on the spectrum assignment algorithm. In Appendix B, we introduce an algorithmic procedure to obtain $\Gamma^{k\pm}_{OSV_{(n,i)}}$ and $m^{k\pm}_{OSV_{(n,i)}}$, as well as the GBE of each state for the WCSA-FF and WCSA-RF operation modes. Note that $\Omega^{WCSA}_{(C,K)}$ of the RF and FF methods are the same.

After obtaining the GBE of all states and considering the normalization equation, we need to solve a linear system of the form $Ax=b$, where A is the transition intensity matrix, x is the vector of steady-state probabilities, and $b=[1,0,0,...,0]^T$. The solution of this linear system for small values of C is easily obtained with direct method (by multiplying b with inverse of A). However, the size of A is exponentially increasing with C. Hence, calculating the exact solution for large C is time consuming and needs huge storage. Therefore, for large C we will propose some approximate solutions in Section V.

B. Operation model of a stand alone EON node without CSA constraint

It has been supposed that in EONs the CSA constraint is necessary and the operation scenario without the CSA constraint is practically complicated. However, recently proposed multi-flow bandwidth variable transponders [22] can

technologically realize the implementation of EON without the CSA constraint. Hence, in this paper the operation scenarios without CSA constraint (WOCSA-FF and WOCSA-RF) are also investigated.

By splitting a lightpath into multiple sub-signals, the number of spectrum slots increases due to the guard band overhead of each sub-signal. If a lightpath with rate R is split into d sub-signals with rate $\Delta R_1,\ \Delta R_2,\ ...,\Delta R_d$, the number of required spectrum slots is equal to $\sum_{i=1}^{d}\left\lceil\frac{\frac{\Delta R_i}{m}+\Delta G)}{\Delta F}\right\rceil$. Generally, a lightpath with rate R can be split into at most $\left\lceil\frac{R}{m(\Delta F-\Delta G)}\right\rceil$ sub-signals with bandwidth of $\Delta F-\Delta G$, provided that $\Delta G<\Delta F$. In this case, the number of required spectrum slots is also $\left\lceil\frac{R}{m(\Delta F-\Delta G)}\right\rceil$. This implies that for WOCSA scenarios N_f satisfies inequality $\left\lceil\frac{\frac{R}{m}+\Delta G}{\Delta F}\right\rceil\le N_f\le\left\lceil\frac{R}{m(\Delta F-\Delta G)}\right\rceil$. However, the guard band ΔG between neighboring signals, which depends on the operational limitations of the given bandwidth-variable wavelength cross-connect (BV-WXC), may be larger than ΔF. In this case, the upper bound of the aforementioned inequality is not valid. Thus, for $\Delta G>\Delta F$ the number of required spectrum slots can be determined according to the number of sub-signals and their transmission rate, ΔR_i. Recently, in [23] a mixed integer linear programming (MILP) formulation has been introduced to select the number of sub-signals of the WOCSA modes as well as the spectrum width and modulation level of each sub-signal.

Modeling the effect of guard band overhead in the introduced Markov model is not straightforward and increases its complexity. However, in the cases where we have $\Delta G<\Delta F$ and $\left\lceil\frac{\frac{R}{m}+\Delta G}{\Delta F}\right\rceil=\left\lceil\frac{R}{m(\Delta F-\Delta G)}\right\rceil$, we can generalize this Markov model to evaluate the WOSCA operation scenarios.

In the remainder of the paper, we ignore the overhead spectrum due to multiple guard bands in the WOCSA operation. Under this assumption, the GBEs of the Markov chain of WOCSA cases are the same as in (3) for $OSV_{(n,i)}\in\Omega_{(C,K)}^{WOCSA}$, where $\Omega_{(C,K)}^{WOCSA}$ is the set of all possible spectrum patterns in WOCSA-RF and WOCSA-RF operation modes. In Appendix C, the details of obtaining the GBEs of all spectrum patterns in WOCSA-FF and WOCSA-RF operation modes are presented.

C. Performance Evaluation Benchmarks

In our evaluation, we consider the blocking probability (BP) and bandwidth fragmentation ratio (BFR) as the performance metrics. The blocking probability of a class k user in EON node with CSA constraint (BP_k^{WCSA}) is obtained by aggregating the probabilities of all states lacking k contiguous idle slots ($\Gamma_{OSV_{(n,i)}}^{k+}=\emptyset$). Hence, we obtain

$$BP_k^{WCSA}=\underbrace{\sum P(OSV_{(n,i)})}_{\forall OSV_{(n,i)}\in\Omega_{(C,K)}^{WCSA},\ \&\&\Gamma_{OSV_{(n,i)}}^{k+}=\emptyset}. \tag{4}$$

Next, the blocking probability of a class k user in EON node without CSA constraint (BP_k^{WOCSA}) is derived by aggregating the probabilities of all states with less than k idle slots ($E<k$), as follows:

$$BP_k^{WOCSA}=\underbrace{\sum P(OSV_{(n,i)})}_{\forall OSV_{(n,i)}\in\Omega_{(C,K)}^{WOCSA},\ \&\&\ E<k}. \tag{5}$$

It is worthwhile noting that the overall blocking probability is obtained by averaging over the blocking probabilities of all classes via $BP^{WCSA}=\frac{\sum_{i=1}^{K}BP_i^{WCSA}}{K}$ and $BP^{WOCSA}=\frac{\sum_{i=1}^{K}BP_i^{WOCSA}}{K}$ under the equal-probability arrival assumption for different classes.

The bandwidth fragmentation is a challenging phenomenon that refers to the non-aligned and small-sized idle spectra in EON spectrum, which mainly arises due to the variable-bandwidth spectrum assignment and the dynamic and time-varying properties of the assigned spectra. In our evaluation, we measure the bandwidth fragmentation of the given occupied spectrum vector (OSV) as follows:

$$BFR(OSV)=\begin{cases}1-\frac{max(\Delta UOS)}{sum(\Delta UOS)}, & if\ sum(\Delta UOS)>0\\ 0, & if\ sum(\Delta UOS)=0\end{cases} \tag{6}$$

where ΔUOS is a vector denoting the unoccupied spectrum intervals of the given OSV, $max(\Delta UOS)$ indicates the largest idle spectrum interval in ΔUOS, and $sum(\Delta UOS)$ is the summation of the idle spectra. For completeness, it should be noted that there may be other definitions to measure the bandwidth fragmentation, which may yield different values [20]. However, all these definitions have the same basic principle borrowed from the storage fragmentation concept in computers and apply the same quantifying concept of bandwidth fragmentation [20]. We obtain the average bandwidth fragmentation ratio BFR_{av} by using the steady-state probabilities of different spectrum patterns via $BFR_{av}=\sum_{\forall OSV_{(n,i)}\in\Omega_{(C,K)}}BFR(OSV_{(n,i)})P(OSV_{(n,i)})$.

IV. Modeling the Network-Wise Operation of EONs

The network-wise operation of EONs is evaluated by modeling the end-to-end spectrum occupation along the established lightpaths. This model depends on the spectrum conversion capabilities of intermediate nodes. We consider two scenarios with and without spectrum conversion capability (WSC and WOSC). The end-to-end blocking probability (BP_{e-e}) is evaluated along the traversing links of the given lightpath. The BP of the network is obtained by averaging over the BP_{e-e} of all established lightpaths. It is worth mentioning that we assume traffic independency among the links. Our analysis could be modified to consider the blocking effect at intermediate nodes by utilizing the same approach as in the Erlang fixed-point approximation [24]. However, considering the traffic dependency among links would further complicate the calculation of BP_{e-e}. Thus, in this study we consider traffic independency among links of a given lightpath.

In the case of WSC, the end-to-end blocking probability of a class i user along an *H-hop* lightpath ($BP_{e-e(i,H)}^{WSC}$) is obtained as follows:

$$BP_{e-e(i,H)}^{WSC}=1-\prod_{l=1}^{H}(1-BP_{l(i)}), \tag{7}$$

where $BP_{l(i)}$ is the blocking probability of a class i user at the lth link.

In order to derive the end-to-end blocking of a class i user along an H-hop lightpath under the WOSC operation mode ($BP^{WOSC}_{e-e(i,H)}$), first the end-to-end occupied spectrum vector (OSV_{e-e}) of the lightpath is computed, then the blocking probability is obtained by evaluating OSV_{e-e} as the spectrum pattern of a stand-alone node. We calculate OSV_{e-e} of an H-hop lightpath by employing the *spectrum union operation* [9] as follows:

$$OSV_{e-e} = \bigcup_{l=1}^{H} OSV_l, \tag{8}$$

where OSV_l denotes OSV of the lth link. For example, the *spectrum union operation* on a 2-hop lightpath with $OSV_1 = \{(0,3),(6,8)\}$ and $OSV_2 = \{(1,2),(4,5),(7,10)\}$ yields $OSV_{e-e} = \{(0,3),(4,5),(6,10)\}$. Afterwards, $BP^{WOSC}_{e-e(i,H)}$ is computed as

$$BP^{WOSC}_{e-e(i,H)} = \underbrace{\sum P(OSV_{e-e})}_{\forall OSV_{e-e} \in \Omega^{e-e}_{(C,K,H)}, \&\& \Gamma^{i+}_{OSV_{e-e}} = \emptyset}, \tag{9}$$

where $\Omega^{e-e}_{(C,K,H)}$ is the set of all OSV_{e-e} patterns for an H-hop lightpath with C spectrum slots and K classes of users with $P(OSV_{e-e})$ given by

$$P(OSV_{e-e}) = \sum_{\forall OSV \in M} \left(\prod_{h=1}^{H} P(OSV_h) \right), \tag{10}$$

where M is the set of all spectrum patterns that generate the same OSV_{e-e}, and $P(OSV_h)$ is the steady-state probability of OSV_h for a stand-alone node. Finally, overall BP of class i users in a given network topology ($BP_{net(i)}$) is achieved as follows

$$BP_{net(i)} = \sum_{H=1}^{H_{max}} \beta_H BP_{e-e(i,H)} \tag{11}$$

where H_{max} is the hop count of the longest path and β_H denotes the percentage of H-hop paths in a given network topology. This coefficient is obtained by determining lightpath of all possible source-destination pairs in the network topology graph and computing the corresponding percentage.

V. Approximate Models

Obtaining the exact performance metrics for large scale EONs is computationally complicated. Thus, to evaluate the performance of EONs in large scale according to practical values for system parameters (C=300 or 600), we need some relaxation assumptions to reduce the computational complexity. In this section, we present two approximate alternative, refereed to as approximation 1 (App. 1) and 2 (App.2), to evaluate large scale EONs' node- and network-wise operation modes.

A. Approximation 1 (App.1)

In App.1, we propose to obtain the solutions of Eq. (3) by categorizing its states with respect to the number of users in each class. Then, a Markov model regardless of the spectrum patterns can be employed to derive the steady-state probabilities of different n, considering the operation scenario without CSA constraint. In this model, all spectrum patterns have equal probability. It is interesting to point out that this Markov chain is the same as the model introduced for multi-rate loss queues (MRLQs) with C servers, where customers are divided into K classes and a class i user requires i servers. In [21], MRLQs were analyzed and a closed-form formula was presented to obtain the steady-state probabilities of the queues. Considering Kaufman's formula [21], the steady-state probability of the number of active users in EON spectrum (n) is given by

$$P(n) = \frac{1}{G} \prod_{i=1}^{K} \frac{1}{n_i!} \left(\frac{\lambda_i}{\mu_i} \right)^{n_i}, \ \forall n \ if \ \sum_{i=1}^{K} (i \times n_i) < C,$$
$$G = \frac{1}{\underbrace{\sum (P(n))}_{\forall n \ if \ \sum_{i=1}^{K} (i \times n_i) < C}}. \tag{12}$$

We approximate the probabilities of the spectrum patterns in both operation scenarios WCSA and WOCSA by assuming uniform distribution for all patterns with the same vector n. Thus, this assumption yields

$$P_{ap}(OSV_{(n,i)}) = \frac{1}{N_{WOCSA}(n) \times G'} \prod_{i=1}^{K} \frac{1}{n_i!} \left(\frac{\lambda_i}{\mu_i} \right)^{n_i}, \tag{13}$$

where for the WCSA operation scenario we have

$$OSV_{(n,i)} \in \Omega^{WCSA}_{(C,K)}, \ i = 1, ..., N_{WCSA}(n), \ G' = \frac{1}{\underbrace{\sum (P(OSV_{(n,i)}))}_{\forall OSV_{(n,i)} \in \Omega^{WCSA}_{(C,K)}}},$$

and for the case of WOCSA

$$OSV_{(n,i)} \in \Omega^{WOCSA}_{(C,K)}, \ i = 1, ..., N_{WOCSA}(n), \ G' = \frac{1}{\underbrace{\sum (P(OSV_{(n,i)}))}_{\forall OSV_{(n,i)} \in \Omega^{WOCSA}_{(C,K)}}},$$

with $P_{ap}(OSV_{(n,i)})$ denoting the approximation of $P(OSV_{(n,i)})$. Although by employing this approximation we obtained a close-form relation for the probability of each spectrum pattern, deriving BP for large scale problem still is complicated. Because, as C increases the number of n are grown so that calculating (12) is very time consuming and needs huge storage. In this regard, we propose to utilize one-dimensional recursion introduced by Kaufman [21]. In one-dimensional recursion the probability of all patterns that have j occupied slots, $g(j)$ is obtained as follows [21]

$$j \times g(j) = \sum_{i=1}^{K} b_i \left(\frac{\lambda_i}{\mu_i} \right) g(j - b_i) \tag{14}$$

where $g(x)$=0 for $x < 0$ and $\sum_{j=0}^{C} g(j) = 1$. In our definition b_i, the number of slots assigned to a class i user, is i. By using $g(j)$ we can approximate BP of class i users ($BP_i^{App.1}$) as follows:

$$BP_i^{App.1} = \sum_{k=0}^{i-1} g(C-k). \tag{15}$$

where $g(C-k)$ for $0 \le k \le i-1$ denotes the probabilities of states blocking a class i users due to the lack of adequate idle slots. It is worthwhile mentioning that this approximate solution estimates the blocking of WOCSA operation scenarios very well, because in WOSCA modes only the number of idle slots affects BP. On the other hand, this approximation underestimates BP in WSCA cases, because it does not take into account those scenarios in which a class i user is blocked due to the lack of i contiguous idle slots, even though there are i or more disjoint idle slots. Therefore, we can utilize App.1 as a lower bound on the performance of WSCA operation modes.

Finally, App.1 is utilized to estimate the end-to-end blocking probability of an *H-hob* lightpath as follows:

$$BP_{e-e(i)}^{App.1} = 1-(1-BP_i^{App.1})^H, \tag{16}$$

B. Approximate 2 (App.2)

In the second approximation, we model the busy/idle states of the spectrum slots as a binomial distribution by assuming the bandwidth utilization ratio as the probability of slot occupation. Then, we utilize the approach in [18] to calculate the blocking probability in WSCA operation modes. In this approach, the busy/idle status of a spectrum slot is considered the head/tail status of a coin and the total number of spectrum slots is considered the total number of tosses. Hence, the probability of finding at least i continuous idle spectrum slots out of a total of C slots is equivalent to the probability of obtaining at least i continuous heads (or tails) among a C-time tossing event.

Let $f(C,i)$ denote the probability that there are at least i continuous idle spectrum slots out of a total of C slots. For a given bandwidth utilization ratio ρ, $f(C,i)$ is obtained as follows [18]:

$$f(C,i) = \sum_{j=1}^{i-1}\left(f(C-j,i)(1-\rho)\rho^{j-1}\right)+(1-\rho)^i,\ i=1,...,K. \tag{17}$$

We estimate the bandwidth utilization ratio by employing the approximate steady-state probabilities obtained in the former subsection as follows:

$$\rho = \frac{1}{C}\sum_{j=1}^{K} jg(j). \tag{18}$$

Subsequently, we can estimate BP of class i user, $BP_i^{App.2}$ as:

$$BP_i^{App.2} = 1-f(C,i), i=1,...,K. \tag{19}$$

From the network-wise perspective, using this approximation the BP_{e-e} of an *H-hop* lightpath in the operation mode of WSC is derived as:

$$BP_{e-e(i)}^{WSC(App.2)} = 1-(f(C,i))^H. \tag{20}$$

Furthermore, the BP_{e-e} of an *H-hop* lightpath in the case of WOSC is evaluated by utilizing the probability that a slot is busy along all the links ρ^H. Hence, the probability that there are i continuous idle slots in OSV_{e-e} of a lightpath, $f_{e-e}(C,i)$, is obtained as:

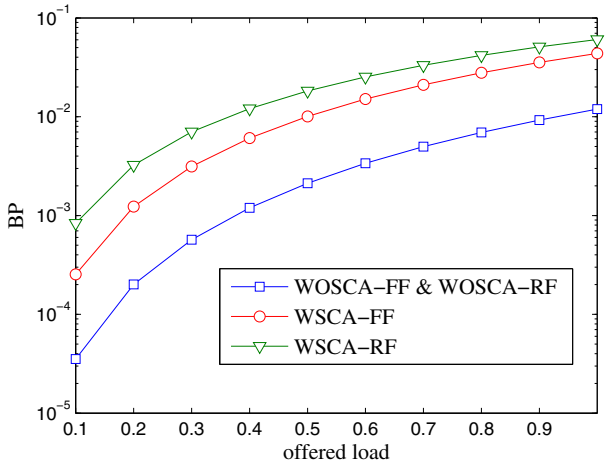

Fig. 3. Blocking probability of different node-wise operation scenarios for C=8, K=3.

$$f_{e-e}(C,i) = \sum_{j=1}^{i-1}\left(f_{e-e}(C-j,i)(1-\rho^H)(\rho^H)^{j-1}\right)+(1-\rho^H)^i, \quad i=1,...,K. \tag{21}$$

Thus, by utilizing $f_{e-e}(C,i)$, we have:

$$BP_{e-e(i)}^{WOSC(App.2)} = 1-f_{e-e}(C,i). \tag{22}$$

VI. Numerical and Simulation Results

A. Results of Node-Wise Modeling

In this subsection, we investigate different node-wise operation scenarios. In Fig. 3, we compare the average BP of the WCSA-FF, WCSA-RF, WOCSA-FF, and WOCSA-RF operation modes. The results are depicted versus *offered load*, which is defined as $\frac{\lambda}{\mu}$, whereby λ is the user arrival rate and μ is the service time of each user. We assume that $\mu_k = \mu$ and $\lambda_k = \frac{\lambda}{K}$ for $k=1,...,K$. Under this assumption, we compute the average BP by ensemble averaging over BP of different classes. Form the figure, we observe that the WCSA-RF mode has the worst BP. Furthermore, BP of WOCSA-FF and WOSCA-FF is the same and lower than that of WSCA-FF. Therefore, in the cases with CSA constraint the spectrum assignment methods, i.e., RF or FF, influence BP. However, in operation scenarios without CSA constraint the spectrum assignment does not affect BP.

The bandwidth fragmentation ratio of different scenarios is compared in Fig. 4. The figure shows that in both WCSA and WOCSA cases the BFR of the RF method is higher than that of FF. Furthermore, by neglecting the CSA constraint the BFR increases. In the WCSA operation modes, the case with higher BFR has also higher BP. On the other hand, although WOCSA-RF has higher BFR than WOCSA-FF, their BP are the same, as shown in Fig. 3. Thus, we can deduce that in WCSA operation modes the growth of BFR increases BP, whereas in the WOSCA operation scenarios such a relation is not valid.

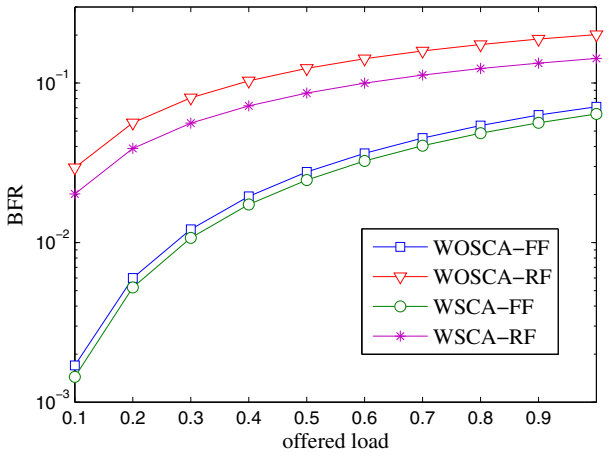

Fig. 4. Bandwidth fragmentation ratio under different node-wise operation scenarios for C=8, K=3.

As discussed, deriving the exact performance of large scale EON operation scenarios is computationally demanding. In Table II, we compare the results of the exact model, denoted as Exact, verifying simulation, indicated as Sim., App.1 and App.2 for small scale cases, (C=6, K=3) and (C=8, K=4), under light and medium offered loads. Furthermore, in Table III, we report the results of verifying simulation, App.1 and App.2 for medium and large scale scenarios, (C=80, K=15), (C=300, K=30), and (C=600, K=50). We simulated different operation scenarios by utilizing an event-driven simulator based on Poisson traffic, i.e., Poisson arrival with parameter λ and exponentially distributed service time with parameter μ. In addition, we assume that incoming traffic is uniformly distributed among K classes, ($\mu_k = \mu$, $\lambda_k = \frac{\lambda}{K}$ for $k = 1, ..., K$). We generated 10^5 and 10^7 arrival events to simulate small and large scale EONs, respectively.

From Table II we observe that the results of the exact model and verifying simulations have the same trend and are close. The closeness between the exact model and verifying simulation implies that we can utilize the results of verifying simulation in the large scale problem as a benchmark to verify the approximation solutions, when we cannot obtain the result of the exact model for large scale EONs. Table II shows that the result of App.1 and the exact model for the WOSCA-RF and WOSCA-FF match very well. However, the BP computed with App.1 is higher than that achieved with the exact model for WSCA-FF and WSCA-RF. As pointed out in Section IV, App.1 underestimates the BP performance of operation modes with CSA constraint. Thus, App.1 can be considered a lower bound for WSCA-FF and WCSA-RF. Interestingly, Table III indicates that the results of App.1 and verifying simulations for the WOSCA-RF and WOSCA-FF modes in large scale scenarios are close, too. Thus, it reveals that the accuracy of App.1 is not affected by the system parameters (C and K). Moreover, the results of App.2 for small scale EONs estimate BP of WSCA operation modes, which is higher than the BP of WOSCA cases. In the large scale EON, the accuracy of App.2 is degraded with the increase of C. Therefore, App.2 is appropriate only for small scale node-wise operation evaluations.

TABLE IV
THE COMPUTATIONAL RUN TIME OF DIFFERENT SOLUTIONS (*msec*).

C=6, K=3			
	Exact	App.1	App.2
WSCA-FF	6.4	0.0064	0.0072
WSCA-RF	6.3		
WOSCA-FF	31.1		
WOSCA-RF	22.2		
C=8, K=4			
	Exact	App.1	App.2
WSCA-FF	115.3	0.0013	0.0069
WSCA-RF	108.2		
WOSCA-FF	3717.1		
WOSCA-RF	2366.7		
	App.1	App.2	
C=300, K=30	0.029	4.7	
C=600, K=50	0.28	21.2	

The computational run time of different solutions is given in Table IV. The results are obtained using a PC with AMD FX Eight-Core 3.1 GHz processor with 8GB RAM. We observe that the run time of the exact solution increases exponentially with respect to C. In addition, the complexity of App.1 and App.2 is less than that of the exact model.

B. Results of Network-Wise Modeling

In this subsection, we first evaluate BP_{e-e} of a 2-*hop* lightpath by utilizing the exact and approximation models and verifying simulations for small scale parameters. Then, the average network-wise BP of different operation modes are evaluated over the well known NSFNET topology for medium and large scale parameters by employing the approximation solutions and verifying simulations. The network-wise EON scenarios are simulated by developing an event-driven simulator. The EON simulator generates Poisson traffic and serves lightpath requests one-by-one by using Dijkstra shortest-path algorithm, where source and destination of a given lighpath are randomly chosen among all network topology nodes. The number of required spectrum slots of each lightpath is randomly selected within [1, K]. The results of the simulations are achieved by generating 10^7 arrival events. Similarly to the former subsection, here we report the average BP_{e-e}, which is obtained by assuming uniform traffic for different classes and ensemble averaging over BP of all classes.

Table V indicates the average BP_{e-e} of a 2-*hop* lightpath for C=5 and K=2 under light and medium offered loads. We observe that with the spectrum conversion capability and ignoring the CSA constraint BP_{e-e} is improved. As expected, the WCS-WOSCA-FF and WCS-WOSCA-RF cases have the same and lowest BP_{e-e}. Whereas the WOCS-WSCA-RF case exhibits the worst BP_{e-e}. This is due to the fact that the random spectrum selection in the RF method increase the BFR (as shown in Fig. 4) and as a result the lack of spectrum conversion capability and the restriction of CSA constraint further increase blocking. The verifying simulation results and exact model have the same trend and are close. Furthermore, the results of both approximations are close to the exact model. It is noteworthy that the run time of the network-wise models have almost the same order of their usage for the node-wise

TABLE II
THE BP OF DIFFERENT NODE-WISE OPERATION SCENARIOS FOR SMALL SCALE EONS.

Operation scenarios	C=6, K=3							
	offered load=0.1				offered load=0.6			
	Exact	Sim.	App.1	App.2	Exact	Sim.	App.1	App.2
WSCA-FF	2.2×10^{-3}	2.7×10^{-3}	1.7×10^{-3}	2.1×10^{-3}	5.4×10^{-2}	5.4×10^{-2}	4.6×10^{-2}	6.2×10^{-2}
WSCA-RF	8.9×10^{-3}	8.2×10^{-3}			7.5×10^{-2}	7.5×10^{-2}		
WOSCA-FF	1.3×10^{-3}	1.8×10^{-3}			3.2×10^{-2}	4.6×10^{-2}		
WOSCA-RF	1.2×10^{-3}	1.8×10^{-3}			3.2×10^{-2}	4.6×10^{-2}		
Operation scenarios	C=8, K=4							
	offered load=0.1				offered load=0.6			
	Exact	Sim.	App.1	App.2	Exact	Sim.	App.1	App.2
WSCA-FF	1.9×10^{-3}	1.7×10^{-3}	1.4×10^{-3}	2.5×10^{-3}	4.9×10^{-2}	4.9×10^{-2}	4×10^{-2}	7.3×10^{-2}
WSCA-RF	9×10^{-3}	9×10^{-3}			7.2×10^{-2}	7.2×10^{-2}		
WOSCA-FF	1×10^{-3}	1.4×10^{-3}			2.8×10^{-2}	4×10^{-2}		
WOSCA-RF	1×10^{-3}	1.4×10^{-3}			2.8×10^{-2}	4×10^{-2}		

TABLE III
THE BP OF DIFFERENT NODE-WISE OPERATION SCENARIOS FOR MEDIUM AND LARGE SCALE EONS.

Operation scenarios	C=80, K=15					
	offered load=0.8			offered load=2.8		
	Sim.	App.1	App.2	Sim.	App.1	App.2
WSCA-FF	1.6×10^{-5}	4.6×10^{-6}	4.3×10^{-3}	8.1×10^{-3}	3.3×10^{-3}	3×10^{-1}
WSCA-RF	3.3×10^{-4}			2.2×10^{-2}		
WOSCA-FF	2.6×10^{-6}			3.4×10^{-3}		
WOSCA-RF	6.5×10^{-6}			3.4×10^{-3}		
Operation scenarios	C=300, K=30					
	offered load=3			offered load=5		
	Sim.	App.1	App.2	Sim.	App.1	App.2
WSCA-FF	1.4×10^{-6}	1.6×10^{-7}	1.8×10^{-1}	2.7×10^{-3}	5.9×10^{-4}	6.8×10^{-1}
WSCA-RF	1.4×10^{-4}			1.3×10^{-2}		
WOSCA-FF	1×10^{-7}			6×10^{-4}		
WOSCA-RF	1.3×10^{-7}			5.8×10^{-4}		
Operation scenarios	C=600, K=50					
	offered load=5			offered load=7		
	Sim.	App.1	App.2	Sim.	App.1	App.2
WSCA-FF	3×10^{-6}	4.3×10^{-7}	5.5×10^{-1}	1.9×10^{-4}	2.2×10^{-5}	6.8×10^{-1}
WSCA-RF	3×10^{-4}			2.9×10^{-3}		
WOSCA-FF	2×10^{-7}			2×10^{-5}		
WOSCA-RF	8×10^{-7}			1.9×10^{-5}		

models, as listed in Table IV. However, the complexity of the exact network-wise model increases exponentially versus $C \times H$, instead of C in the case of node-wise model.

The results of simulations and approximate models for medium and large scale cases are given in Table VI. In this table we can see the same trend as in the results of Table V. Here, for large scale scenarios the benefit of spectrum conversion capability is further pronounced. In the case of C=300, K=30, and offered load=3, for example,the BP of the WOCS-WCSA-FF is 2.3×10^{-4}, which is reduced to 5.4×10^{-5} by utilizing spectrum conversion in the case of WSC-WCSA-FF. Furthermore, the first and second approximations give a lower and upper estimations of the simulation results, respectively. The results of App.1 for three values of (C, K) have the same trend with respect to the verifying simulation. The accuracy of App.1 is not degraded with increase of C and K. On the other hand, although App.2 gives an upper bound of the simulation results, with growing C and K its accuracy is degraded. Thus, App.2 is applicable only for small scale cases ($C < 80$).

VII. CONCLUSIONS

In this paper, we have analyzed the exact node-wise and network-wise operation scenarios in EONs. Four operation scenarios have been investigated in the node-wise performance evaluation, which are determined based on the spectrum allocation methods (FF or RF) and the status of assignment constraint (WCSA or WOCSA). We presented an algorithmic procedure to derive the global balance equations of the corresponding Markov chains for all operation scenarios. Furthermore, the network-wise operation was evaluated by analyzing the end-to-end blocking probability for eight operation modes. In order to reduce the computational complexity, we also presented two approximate solutions to obtain the steady-state probabilities of Markov models and the end-to-end blocking probability. The results of the exact models, approximations, and verifying simulations were compared. Our comparison reveals that the exact model and simulation have the same trend and are close. In addition, the accuracy of both approximations is acceptable. The approximate solutions are also examined under large scale scenarios by considering the simulation results as a benchmark. The accuracy of the first approximation is not degraded in large scale cases, as opposed to the second one, which is only applicable to small scale problems.

TABLE V
THE AVERAGE BP_{e-e} OF DIFFERENT NETWORK-WISE OPERATION SCENARIOS FOR A SMALL SCALE 2-*hop* PATH.

Operation scenarios	C=5, K=2, H=2							
	offered load=0.2				offered load=0.6			
	Exact	Sim.	App.1	App.2	Exact	Sim.	App.1	App.2
WOSC-WSCA-FF	6.1×10^{-3}	3.5×10^{-3}	5.3×10^{-3}	8.7×10^{-3}	5.6×10^{-2}	2.9×10^{-2}	4.8×10^{-2}	8.2×10^{-2}
WOSC-WSCA-RF	1.1×10^{-2}	5.2×10^{-3}			8.1×10^{-2}	3.4×10^{-2}		
WOSC-WOSCA-FF	2.3×10^{-3}	3.1×10^{-3}			2.9×10^{-2}	2.6×10^{-2}		
WOSC-WOSCA-RF	4.2×10^{-3}	3.4×10^{-3}			4.4×10^{-2}	2.8×10^{-2}		
WSC-WSCA-FF	5.9×10^{-3}	2.6×10^{-3}		4.2×10^{-3}	5.4×10^{-2}	2.2×10^{-2}		4.1×10^{-2}
WSC-WSCA-RF	9.7×10^{-3}	4.2×10^{-3}			7×10^{-2}	2.8×10^{-2}		
WSC-WOSCA-FF	2.1×10^{-3}	2.1×10^{-3}			2.3×10^{-2}	1.9×10^{-2}		
WSC-WOSCA-RF	2.1×10^{-3}	2.2×10^{-3}			2.3×10^{-2}	1.9×10^{-2}		

TABLE VI
THE AVERAGE BP OF NSFNET TOPOLOGY UNDER DIFFERENT OPERATION SCENARIOS FOR MEDIUM AND LARGE SCALE PARAMETERS.

Operation scenarios	C=80, K=15					
	offered load=0.8			offered load=2.8		
	Sim.	App.1	App.2	Sim.	App.1	App.2
WOSC-WSCA-FF	1.5×10^{-4}	6.6×10^{-6}	1×10^{-1}	5.2×10^{-3}	2.6×10^{-4}	3.2×10^{-1}
WOSC-WSCA-RF	1.8×10^{-3}			1.5×10^{-2}		
WOSC-WOSCA-FF	3.3×10^{-5}			1.2×10^{-3}		
WOSC-WOSCA-RF	4.5×10^{-5}			1.8×10^{-3}		
WSC-WSCA-FF	8.4×10^{-5}		6.6×10^{-3}	2.5×10^{-3}		1×10^{-1}
WSC-WSCA-RF	9.4×10^{-4}			9.8×10^{-3}		
WSC-WOSCA-FF	3×10^{-5}			9.6×10^{-4}		
WSC-WOSCA-RF	2.9×10^{-5}			9.8×10^{-4}		
Operation scenarios	C=300, K=30					
	offered load=3			offered load=5		
	Sim.	App.1	App.2	Sim.	App.1	App.2
WOSC-WSCA-FF	2.3×10^{-4}	3.9×10^{-7}	5.1×10^{-1}	2.9×10^{-3}	7.6×10^{-6}	6.2×10^{-1}
WOSC-WSCA-RF	3.4×10^{-3}			1.4×10^{-2}		
WOSC-WOSCA-FF	1.1×10^{-5}			2.7×10^{-4}		
WOSC-WOSCA-RF	2.6×10^{-5}			4.7×10^{-4}		
WSC-WSCA-FF	5.4×10^{-5}		2.8×10^{-1}	8.6×10^{-4}		4.3×10^{-1}
WSC-WSCA-RF	1.1×10^{-3}			5.7×10^{-3}		
WSC-WOSCA-FF	7.8×10^{-6}			1.6×10^{-4}		
WSC-WOSCA-RF	7.7×10^{-6}			1.5×10^{-4}		
Operation scenarios	C=600, K=50					
	offered load=5			offered load=8		
	Sim.	App.1	App.2	Sim.	App.1	App.2
WOSC-WSCA-FF	9.4×10^{-4}	4.1×10^{-7}	7.3×10^{-1}	2.8×10^{-2}	2.2×10^{-4}	8.4×10^{-1}
WOSC-WSCA-RF	8.6×10^{-3}			5.4×10^{-2}		
WOSC-WOSCA-FF	4.5×10^{-5}			6.6×10^{-3}		
WOSC-WOSCA-RF	1.1×10^{-4}			9.3×10^{-3}		
WSC-WSCA-FF	2.2×10^{-4}		5.8×10^{-1}	1.3×10^{-2}		7.5×10^{-1}
WSC-WSCA-RF	3.1×10^{-3}			3.3×10^{-2}		
WSC-WOSCA-FF	3.2×10^{-5}			4.3×10^{-3}		
WSC-WOSCA-RF	2.9×10^{-5}			4.3×10^{-3}		

APPENDIX A
SORTING AND NUMBERING THE BANDWIDTH OCCUPATION PATTERNS IN OPERATION SCENARIOS WCSA-FF AND WCSA-RF

In this appendix, we present a procedure to sort and number the spectrum patterns in a EON node with CSA constraint, which helps us algorithmically derive the GBEs of the corresponding Markov model. Toward this end, we categorize the spectrum patterns with respect to the number of served users. Let N denote the number of users, $N=\sum_{i=1}^{K} n_i$, then sort the spectrum patterns in ascending order with respect to N. For a given N, all possible vectors n are obtained by considering all the solutions of the following equation:

$$n_1+n_2+...+n_K=N_j$$
$$s.t.,\ n_1+2n_2+3n_3+...+Kn_K\le C,$$
$$\&\&\ 0\le n_i,\ \&\&\ 0\le N_j\le C. \qquad \text{(A-1)}$$

The solutions of the above linear equation are sorted in ascending order with respect to the value of n_K. The solutions with the same n_K are sorted in ascending order versus the value of n_{K-1}, and in the cases that n_K and n_{K-1} are the same, they are aligned in ascending order with respect to the value of n_{K-2}, and so on.

After obtaining all vectors n that satisfy Eq. (A-1) for $N=0,...,C$, we determine all the possible spectrum patterns of each vector. The number of spectrum patterns of each vector n is given by Eq. (1a). These patterns are sorted with respect to the permutation of the classes of users. For a given n, all the possible patterns are obtained by considering all the permutations of the idle and busy slots. We can determine all permutations of the empty slots using the following linear

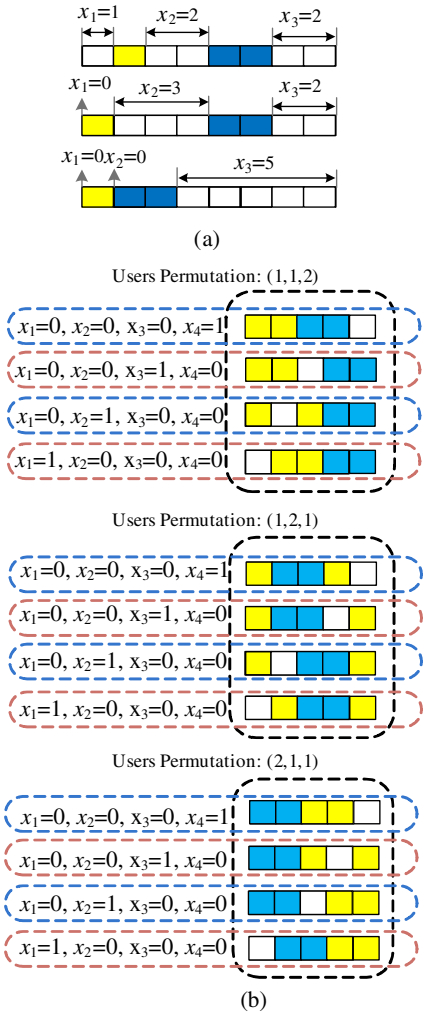

Fig. 5. (a) Some permutations of idle slots, (b) categorizing and arrangement of the occupation patterns for n=(2,1,0), C=5, and K=3.

equation:

$$x_1+x_2+\ldots+x_{N+1}=E,\ s.t.,\ E=C-\sum_{i=1}^{K}(i\times n_i),\ \&\&\ 0\le x_i, \tag{A-2}$$

where x_i indicates the number of idle slots between the $(i-1)$th and ith busy slots, as shown in Fig. 5(a). For each solution, there are $\frac{N!}{\prod_{i=1}^{K} n_i!}$ distinct permutations for the busy slots, and each of them brings a specific spectrum pattern. To sort the spectrum patterns, first we determine all the possible permutations of the users and obtain the solutions of (A-2). Then, we sort the permutations in ascending order with respect to the class of the first user. In the scenario where the first users are the same, the permutations are sorted with respect to the class of the second user, and so on.

After sorting the permutations by using the solutions of Eq. (A-2), the corresponding spectrum patterns are determined. The patterns of each permutation are sorted with respect to the solutions of Eq. (A-2), which are arranged in ascending order with respect to x_1. In the case that the solutions have the same x_1, they are ordered with respect to x_2, and so on. In Fig. 5(b), we show the categorization and arrangement of the spectrum patterns for $n=(2,\ 1,\ 0)$, $C=5$, and $K=3$. We summarize the described procedure as follows:

- For $N=0,\ldots,C$, find all vectors n satisfying Eq. (A-1) and sort the vectors with respect to N in ascending order (sort the vectors with the same N with respect to the value of n_K).
- For each vector n, determine all the permutations of users and obtain all the solutions of Eq. (A-2).
- Sort the permutations and solutions according to the described procedure (Fig. 5(b)).

After sorting the occupation patterns, we can number the spectrum patterns from 1 to N_T, as shown in Algorithm 1, where N_T is the total number of spectrum patterns.

Algorithm 1: Numbering spectrum patterns

Input : C and K
Output: the sorted and numbered spectrum patterns (S)

1 **Initialization:** $Offset$=0; S=∅;
2 **for** $N=0,\ldots,C$ **do**
3 Find all $n=(n_1,\ldots,n_K)$ that satisfy (A-1);
4 Sort vectors n in ascending order with respect to n_K, n_{K-1},..., n_2;
5 **for** ∀ *the sorted vectors* n **do**
6 Find all spectrum patterns of the given n;
7 Sort the spectrum pattern according to the users' permutation and solutions of (A-2);
8 Number the sorted patterns from $Offset$ to $Offset+N_{WCSA}(n)$;
9 S=S⋃{all the spectrum patterns of the given n};
10 $Offset=Offset+N_{WCSA}$;
11 **end**
12 **end**

It should be noted that the number of solutions of (A-1) for large C may be huge, which restricts this categorization mechanism for large C. However, this technique can be useful to reduce the complexity of the exact solution by employing the aggregation methods introduced in [25] to solve huge Markov chains.

APPENDIX B
GBE DERIVATION IN THE OPERATION SCENARIOS WCSA-FF AND WCSA-RF

In this appendix, we present an algorithmic procedure to derive the GBEs of the Markov model for the operation scenarios WCSA-FF and WSCA-RF. Algorithm 2 represents details of the procedure. The inputs of the algorithm are C and K, and its output is matrix $A_{(N_T\times N_T)}$, where its ith row denotes the GBE of the ith spectrum pattern (OSV_i). In line 1, all the states of the given C and K are sorted and numbered using Algorithm 1. In lines 2-3, matrix A is initialized by setting all the elements of the first row to 1 and the other ones to 0. Note that all elements of the first row are set to 1 in order to satisfy the normalization constraint of the steady-state probabilities. The loop in lines 4-13 determines the GBEs of all states and calculates the non-zero elements of A according to Eq. (2a). In line 5,

function $S\{\cdot\}$ returns the spectrum pattern of the given number, i, according to the introduced categorization algorithm. By using this mechanism, instead of storing all spectrum patterns in a look-up table, we only need to store all solutions of (A-1) and then performing the categorization and sorting procedure. Note that the functions $FindPos\{OSV_i,\ j,\ FF\_RF\}$ and $FindNeg\{OSV_i,\ j\}$ determine all the positive (with the arrival of a class j user) and negative (with the departure of a class j user) transitions of the state OSV_i, respectively, where FF_RF specifies the spectrum allocation method, FF or RF. Furthermore, the function $Size\{\cdot\}$ counts the element of the given set. The details of $FindPos\{\cdot\}$ and $FindNeg\{\cdot\}$ are presented in Algorithm 3 and 4, respectively. In these algorithms, the function $FindIndex\{\cdot\}$ determines the index number of the spectrum pattern according to the arrangement of Algorithm 1.

Algorithm 2: GBE derivation

Input : C and K, λ_k and μ_k (k=1,...,K)
Output: The transition matrix $A_{(N_T \times N_T)}$

1 Sort and number all states of the Markov chain using Algorithm 1;
2 Set all elements of the matrix $A_{(N_T \times N_T)}$ to 0;
3 Set all elements of the first row of A to 1;
4 **for** $N_j = 0,...,C$ **do**
5 $\mathrm{OSV}_i = S\{i\}$;
6 **for** $N_j = 0,...,C$ **do**
7 $\Gamma^{j+}_{(OSV_i)} = FindPos\{OSV_i,\ j,\ FF\_RF\}$;
  $\Gamma^{j-}_{(OSV_i)} = FindNeg\{OSV_i,\ j,\ FF\_RF\}$;
8 $m^{j+}_{(OSV_i)} = Size\{\Gamma^{j+}_{(OSV_i)}\}$; $m^{j-}_{(OSV_i)} = Size\{\Gamma^{j-}_{(OSV_i)}\}$;
9 $A(i,i) = A(i,i) + \mu_j + m^{j-}_{(OSV_i)}\mu_j$;
10 $\forall u \in \Gamma^{j+}_{(OSV_i)}$ set $A(i,u) = -\mu_j$;
11 **for** $\forall t \in \Gamma^{j-}_{(OSV_i)}$ **do**
12 $\Gamma^{j+}_{(OSV_t)} = FindPos\{OSV_t,\ j\}$;
  $m^{j+}_{(OSV_t)} = Size\{\Gamma^{j+}_{(OSV_t)}\}$; $A(i,t) = \frac{-\lambda_j}{m^{j+}_{(OSV_t)}}$;
13 **end**
14 **end**
15 **end**

APPENDIX C
GBE DERIVATION IN THE OPERATION SCENARIOS WOCSA-FF AND WOCSA-RF

In order to derive the GBEs of the Markov chain for the WOCSA-FF and WOCSA-RF cases, first we sort and number all the possible spectrum patterns according to Algorithm 1. It should be noted that for these cases the relation applied in line 7 of Algorithm 1, (A-2) is modified as follows:

$$x_1 + x_2 + ... + x_{N_S+1} = E,\ s.t.,\ E = C - \sum_{i=1}^{K} (i \times n_i),\ \&\&\ 0 \le x_i, \tag{A-3}$$

where N_S is the number of busy slots ($N_S = \sum_{i=1}^{K} (i \times n_i)$). Furthermore, $N_{WCSA}(n)$ in lines 8 and 10 of Algorithm 1 is replaced with $N_{WOCSA}(n)$. We can utilize Algorithm 2 as well as the modified versions of Algorithm 3 and 4 to derive the GBEs of WOCSA-FF and WOCSA-RF operation modes. In order to obtain $\Gamma^{k+}_{OSV_t}$ in the WOCSA-FF scenario, $SelectInterval$ in line 2 of Algorithm 3 is set to the first available j slots (neglecting the contiguous constraint). Similarly, for the case of WOCSA-RF, line 10 of Algorithm 3 is changed by setting ΔUSV_j as the set of all scenarios to select j idle slots out of available idle slots. In addition, Algorithm 4 can be used for the WOCSA cases by changing the contiguous interval $(f_L,\ f_U)$ into a non-contiguous set $\{f_L,...,f_U\}$, which specifies all slots assigned to a lightpath.

Algorithm 3: $FindPos\{OSV_i,\ j,\ FF\_RF\}$

Input : OSV_i, j, FF_RF
Output: $\Gamma^{j+}_{(OSV_t)}$

1 **if** FF_RF=FF **then**
2 $SelectInterval$= the first available j contiguous idle slots of OSV_i;
3 **if** $SelectInterval \neq \emptyset$ **then**
4 $OSV_{new} = OSV_i \bigcup SelectInterval$;
  $u = FindIndex\{OSV_{new}\}$; $\Gamma^{+j}_{OSV_i} = \{u\}$;
5 **else if** $SelectInterval = \emptyset$ **then**
6 $\Gamma^{+j}_{OSV_i} = \{\emptyset\}$;
7 **end**
8 **else if** FF_RF=RF **then**
9 $\Gamma^{+j}_{OSV_i} = \{\emptyset\}$;
10 ΔUSV_j=all available j contiguous idle slots in OSV_i;
11 **for** $\forall$ $SelectInterval \in \Delta USV_j$ **do**
12 $OSV_{new} = OSV_i \bigcup SelectInterval$;
  $u = FindIndex\{OSV_{new}\}$; $\Gamma^{+j}_{OSV_i} = \Gamma^{+j}_{OSV_i} \bigcup \{u\}$;
13 **end**
14 **end**

Algorithm 4: $FindNeg\{OSV_i,\ j\}$

Input : OSV_i and j
Output: $\Gamma^{j-}_{(OSV_t)}$

1 $\Gamma^{-j}_{OSV_i} = \{\emptyset\}$;
2 **for** $\forall (f_L, f_U) \in OSV_i$ $\&\&(f_U - f_L) = j$ **do**
3 $OSV_{new} = OSV_i - \{(f_L, f_U)\}$; $u = FindIndex\{OSV_{new}\}$;
4 $\Gamma^{-j}_{OSV_i} = \Gamma^{-j}_{OSV_i} \bigcup \{u\}$;
5 **end**

REFERENCES

[1] M. Jinno, H. Takara, B. Kozicki, Y. Tsukishima, Y. Sone, and S. Matsuoka, "Spectrum-efficient and scalable elastic optical path network: Architecture, benefits, and enabling technologies," *IEEE Commun. Mag.*, vol. 47, no. 11, pp. 66–73, Nov. 2009.

[2] W. Shi, Z. Zhu, M. Zhang, and N. Ansari, "On the effect of bandwidth fragmentation on blocking probability in elastic optical networks," *IEEE Trans. Commun.*, vol. 61, no. 7, pp. 2970–2978, July 2013.

[3] C.-F. Hsu and F.-S. Lin, "On dynamic wavelength assignment in wavelength-convertible multi-granular optical networks," *IEEE Trans. Commun.*, vol. 57, no. 8, pp. 2221–2224, Aug. 2009.

[4] O. Gerstel, M. Jinno, A. Lord, and S. J. Ben Yoo, "Elastic optical networking: a new dawn for the optical layer?" *IEEE Commun. Mag.*, vol. 50, no. 2, pp. S12–S20, Feb. 2012.

[5] M. Jinno, B. Kozicki, H. Takara, A. Watanabe, Y. Sone, T. Tanaka, and A. Hirano, "Distance-adaptive spectrum resource allocation in spectrum-sliced elastic optical path network," *IEEE Commun. Mag.*, vol. 48, no. 8, pp. 138–145, Aug. 2010.
[6] K. Christodoulopoulos, I. Tomkos, and E. Varvarigos, "Elastic bandwidth allocation in flexible OFDM-based optical networks," *IEEE/OSA J. Lightw. Technol.*, vol. 29, no. 9, pp. 1354–1366, May 2011.
[7] M. Klinkowski and K. Walkowiak, "Routing and spectrum assignment in spectrum sliced elastic optical path network," *IEEE Commun. Lett.*, vol. 15, no. 8, pp. 884–886, Aug. 2011.
[8] K. Christodoulopoulos, I. Tomkos, and E. Varvarigos, "Dynamic bandwidth allocation in flexible OFDM-based networks," in *Proc. 2011 Opt. Fiber Comm. Conf.*, paper OTuI5.
[9] X. Wan, N. Hua, and X. Zheng, "Dynamic routing and spectrum assignment in spectrum-flexible transparent optical networks," *IEEE/OSA J. Opt. Commun. Netw.*, vol. 4, no. 8, pp. 603–613, Aug. 2012.
[10] M. Klinkowski, M. Ruiz, L. Velasco, D. Careglio, V. Lopez, and J. Comellas, "Elastic spectrum allocation for time-varying traffic in flexgrid optical networks," *IEEE J. Sel Areas Commun.*, vol. 30, no. 1, pp. 26–38, Jan. 2013.
[11] K. Christodoulopoulos, I. Tomkos, and E. Varvarigos, "Time-varying spectrum allocation policies and blocking analysis in flexible optical networks," *IEEE J. Sel. Areas Commun.*, vol. 30, no. 1, pp. 1–13, Jan. 2013.
[12] R. Ramaswami and K. N. Sivarajan, "Routing and wavelength assignment in all-optical networks," *IEEE/ACM Trans. Netw.*, vol. 3, no. 5, pp. 489–500, Oct. 1995.
[13] D. J. Geisler, R. Proietti, Y. Yin, R. P. Scott, X. Cai, N. K. Fontaine, L. Paraschis, O. Gerstel, and S. J. B. Yoo, "Experimental demonstration of flexible bandwidth networking with real-time impairment awareness," *OSA Opt. Exp.*, vol. 19, no. 26, pp. B736–B745, Dec. 2011.
[14] X. Cai, K. Wen, R. Proietti, Y. Yin, D. J. Geisler, R. P. Scott, C. Qin, L. Paraschis, O. Gerstel, and S. J. B. Yoo, "Experimental demonstration of adaptive combinational QoT degradation restoration in elastic optical networks," *IEEE/OSA J. Lightw. Technol.*, vol. 31, no. 4, pp. 664–671, Feb. 2013.
[15] K. Wen, X. Cai, Y. Yin, D. J. Geisler, R. Proietti, R. P. Scott, N. K. Fontaine, and S. J. B. Yoo, "Adaptive spectrum control and management in elastic optical networks," *IEEE J. Sel. Areas Commun.*, vol. 30, no. 1, pp. 39–48, Jan. 2013.
[16] S. Yang and F. Kuipers, "Impairment-aware routing in translucent spectrum-sliced elastic optical path networks," in *Proc. 2012 Eur. Conf. Netw. Opt. Comm.*, pp. 1–6.
[17] H. Beyranvand and J. A. Salehi, "A quality-of-transmission aware dynamic routing and spectrum assignment scheme for future elastic optical networks," *IEEE/OSA J. Lightw. Technol.*, vol. 31, no. 18, pp. 3043–3054, Sept. 15, 2013.
[18] L. Peng, C.-H. Youn, and C. Qiao, "Theoretical analyses of lightpath blocking performance in CO-OFDM optical networks with/without spectrum conversion," *IEEE Commun. Lett.*, vol. 17, no. 4, pp. 789–792, Apr. 2013.
[19] Y. Yu, J. Zhang, Y. Zhao, X. Cao, X. Lin, and W. Gu, "The first single-link exact model for performance analysis of flexible grid WDM networks," in *Proc. 2013 Opt. Fiber Comm. Conf.*, paper JW2A.68.
[20] Z. Zhu, W. Lu, L. Zhang, and N. Ansari, "Dynamic service provisioning in elastic optical networks with hybrid single-/multi-path routing," *IEEE/OSA J. Lightw. Technol.*, vol. 31, no. 1, pp. 15–22, Jan. 2013.
[21] J. S. Kaufman, "Blocking in a shared resource environment," *IEEE Trans. Commu.*, vol. 29, no. 10, pp. 1474–1481, Oct. 1981.
[22] M. Jinno, H. Takara, Y. Sone, K. Yonenaga, and A. Hirano, "Multiflow optical transponder for efficient multilayer optical networking," *IEEE Commun. Mag.*, vol. 50, no. 5, pp. 56-65, May 2012.
[23] A. Pagès, J. Perelló, S. Spadaro, and J. Comellas, "Optimal route, spectrum, and modulation level assignment in split-spectrum-enabled dynamic elastic optical networks," *IEEE/OSA J. Opt. Commun. Netw.*, vol. 6, no. 2, pp. 114–126, Feb. 2014.
[24] F. P. Kelly, "Fixed point models of loss networks," *J. Australian Mathematical Society*, Series B. Applied Mathematics, vol. 31, no. 2, pp. 204–218, Oct. 1989.
[25] G. Bolch, S. Greiner, H. Meer, and K. Trivedi, *Queueing Networks and Markov Chains: Modeling and Performance Evaluation with Computer Science Applications*, 2nd ed. John Wiley and Sons Ltd., 2006.

Hamzeh Beyranvand was born in Khorramabad, Iran, on June 27, 1984. He received the B.S. degree (with honor, first rank) in electrical engineering from Shahed University, Tehran, Iran in 2006 and the M.S. degree in Sharif University of Technology (SUT), Tehran, Iran in 2008. He is currently working toward the Ph.D. degree in the Department of Electrical Engineering at SUT. His research interests are in the areas of optical CDMA systems, optical OFDMA-based elastic bandwidth networks, GMPLS network, QoS provisioning in optical networks, queuing theory, Fiber-Wireless (FiWi) networks.

Martin Maier is a full professor with the Institut National de la Recherche Scientifique (INRS), Montreal, Canada. He was educated at the Technical University of Berlin, Germany, and received MSc and PhD degrees (both with distinctions) in 1998 and 2003, respectively. In the summer of 2003, he was a postdoc fellow at the Massachusetts Institute of Technology (MIT), Cambridge. He was a visiting professor at Stanford University, Stanford, October 2006 through March 2007. Dr. Maier is a co-recipient of the 2009 IEEE Communications Society Best Tutorial Paper Award and Best Paper Award presented at The International Society of Optical Engineers (SPIE) Photonics East 2000-Terabit Optical Networking Conference. He is the founder and creative director of the Optical Zeitgeist Laboratory (www.zeitgeistlab.ca). He is the author of the book *Optical Switching Networks* (Cambridge University Press, 2008), which was translated into Japanese in 2009 and the lead author of the book *FiWi Access Networks* (Cambridge University Press, 2012).

Jawad A. Salehi (M'84–SM'07–FM'10) was born in Kazemain, Iraq, on December 22, 1956. He received the B.S. degree from the University of California, Irvine, in 1979, and the M.S. and Ph.D. degrees from the University of Southern California (USC), Los Angeles, in 1980 and 1984, respectively, all in electrical engineering. He is currently a Full Professor at the Optical Networks Research Laboratory (ONRL), Department of Electrical Engineering, Sharif University of Technology (SUT), Tehran, Iran. From 1981 to 1984, he was a Full-Time Research Assistant at the Communication Science Institute, USC. From 1984 to 1993, he was a Member of Technical Staff of the Applied Research Area, Bell Communications Research (Bellcore), Morristown, NJ. Prof. Salehi was an Associate Editor for Optical CDMA of the IEEE TRANSACTIONS ON COMMUNICATIONS since 2001 to 2012. He is among the 250 preeminent and most influential researchers worldwide in the Institute for Scientific Information (ISI) Highly Cited in the Computer-Science Category.